OPTICA

Quantum phase modulation with acoustic cavities and quantum dots

Poolad Imany,[1,2,3,†] Zixuan Wang,[1,2,†] Ryan A. DeCrescent,[1] Robert C. Boutelle,[1] Corey A. McDonald,[1,2] Travis Autry,[1] Samuel Berweger,[1] Pavel Kabos,[1] Sae Woo Nam,[1] Richard P. Mirin,[1] and Kevin L. Silverman[1,4]

[1]National Institute of Standards and Technology, Boulder, Colorado 80305, USA
[2]Department of Physics, University of Colorado, Boulder, Colorado 80309, USA
[3]e-mail: Poolad.imany@nist.gov
[4]e-mail: Kevin.silverman@nist.gov

Received 20 December 2021; revised 31 March 2022; accepted 4 April 2022; published 29 April 2022

Fast, efficient, and low-power modulation of light at microwave frequencies is crucial for chip-scale classical and quantum processing as well as for long-range networks of superconducting quantum processors. A successful approach to bridge the gap between microwave and optical photons has been to use intermediate platforms, such as acoustic waves, that couple efficiently to a variety of quantum systems. Here, we use gigahertz-frequency focusing surface acoustic wave cavities on GaAs that are piezo-electrically coupled to superconducting circuits and parametrically coupled, via strain, to photons scattered from InAs quantum dots. We demonstrate modulation of single photons with a half-wave voltage as low as 44 mV, and subnatural modulation sideband linewidths. These demonstrations pave the way for efficient and low-noise transduction of quantum information between microwave and optical domains.

https://doi.org/10.1364/OPTICA.451418

Electro-optical modulation spans many classical and quantum applications such as high-speed optical data transmission [1,2] and quantum transduction of information between light and matter qubits [3,4]. Focusing on the quantum realm, transduction is a key element for long-range networks of superconducting quantum processors. Quantum information encoded in microwave photons must be preserved at millikelvin temperatures to be protected against thermal noise, making long-range transmission infeasible. Optical quantum information, on the other hand, can be preserved at room temperature and transmitted over long distances with minimal loss and decoherence via optical fiber or free space.

An outstanding challenge for microwave-to-optical conversion of photons arises from the energy (frequency) difference between these two domains, exceeding five orders of magnitude. Many platforms have been introduced to mediate these interactions: (1) electro-optic approaches with optical microresonators and superconducting resonators [5]; (2) acoustic intermediates such as photonic–phononic crystals [3,6–8], mechanical membranes [9], and optical microresonators coupled to surface acoustic wave (SAW) resonators [10]; (3) magnons [11]; (4) Rydberg atoms [12]. The approaches that employ acoustics aim to leverage the slower speed of sound compared to light (∼five orders of magnitude). The wavelength of microwave phonons is comparable to optical photons and typically results in more efficient interactions. Indeed, microwave and radiofrequency phonons have been shown to couple strongly to a variety of quantum systems, such as superconducting circuits [3,13], defect centers in diamond [14], and semiconductor quantum dots (QDs) [15–17], and are emerging as universal transducers [18].

Here we parametrically modulate the emission frequency of an InAs QD to encode information stored in a gigahertz focusing SAW resonator onto an optical carrier. The QD is monolithically integrated into the SAW cavity and is sensitive to phonons via the deformation potential [15,17,19]. This platform has many potential advantages over other current strategies. One is the QD's remarkable sensitivity to local strain in the host crystal; for a unit displacement, the exciton energy shift is about two orders of magnitude more sensitive (∼10 GHz/pm) [17] than that of small optical cavities (∼100 MHz/pm) [20]. Also, the entire device (superconducting circuitry, acoustic resonator, QD) can be fabricated on a single GaAs substrate. GaAs is a unique material in that it not only couples SAWs to superconducting circuits piezo-electrically, but also natively hosts InAs QDs. The use of QDs also ensures that only single photons are emitted in a transduction cycle. This platform supports near-critical electro–acoustic coupling, acoustic quality factors higher than 10^4, mode volumes of the order of 10 μm^3, and scattering linewidths below 200 MHz, the lifetime limit of the QD [21]. The development of state-of-the-art SAW cavities and the characteristics of our chosen platform facilitate strong electro-acousto-optic modulation, yielding a half-wave voltage (V_π) of 44 mV, a total photon conversion efficiency of $\eta = 10^{-15}$, and a g_0 of $2\pi \times 42$ kHz. Given the strong sensitivity of our QDs to strain and the potential to continue to shrink cavity mode volumes, we anticipate g_0 values to approach $2\pi \times 10$ MHz with an optimally positioned QD. To put these numbers in perspective, we refer to [4], where a comprehensive summary of different platforms, their coupling rates, and overall photon conversion efficiencies are reported, showing $g_0 = 2\pi \times 1.3$ MHz [7] and $\eta = 47\%$ [9] as the highest numbers to date.

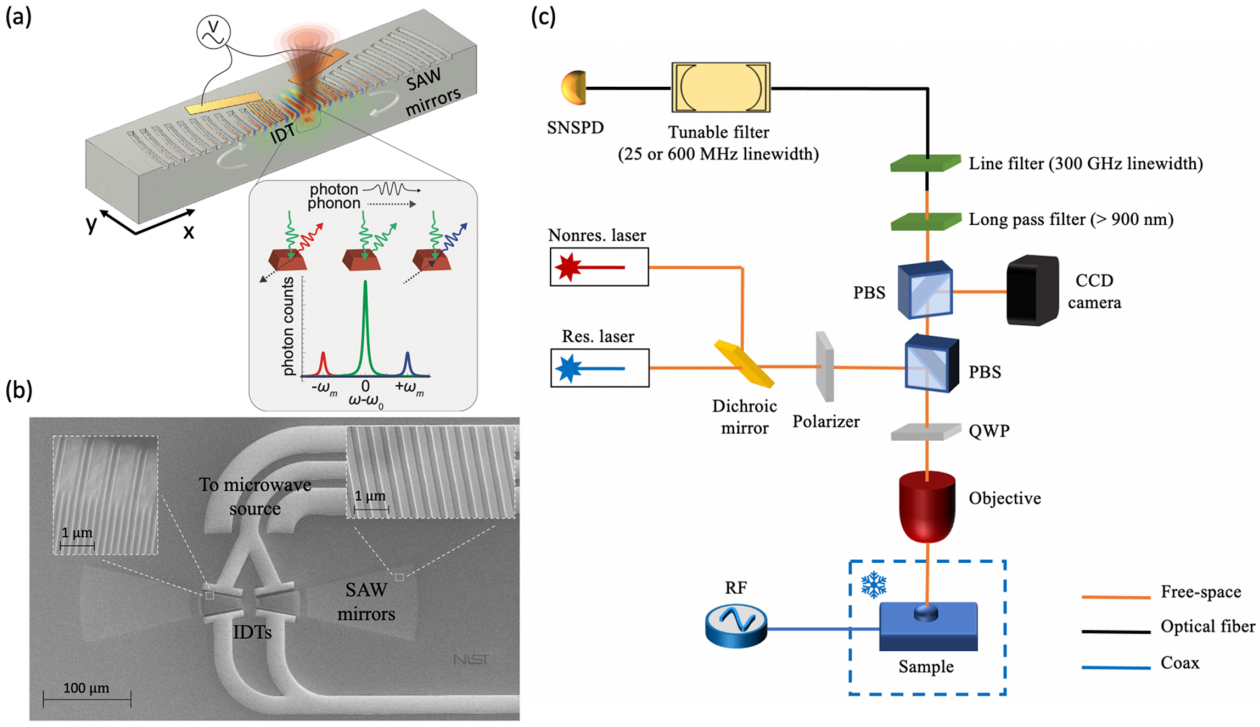

Fig. 1. (a) Illustration of the modulation scheme. An IDT drives a SAW cavity to generate phonons from microwave photons. The phonons interact with optical photons mediated by a QD, generating sidebands in the scattering spectrum. The inset shows three different photon scattering processes: (left) one phonon is emitted; (middle) no phonon is involved; (right) one phonon is absorbed. The x axis for the inset is centered at the QD transition. (b) Scanning electron microscopy image of the fabricated device. (c) Experimental setup. PBS, polarizing beam splitter; QWP, quarter-wave plate; RF, radio frequency; CCD, charge-coupled device; SNSPD, superconducting nanowire single-photon detector.

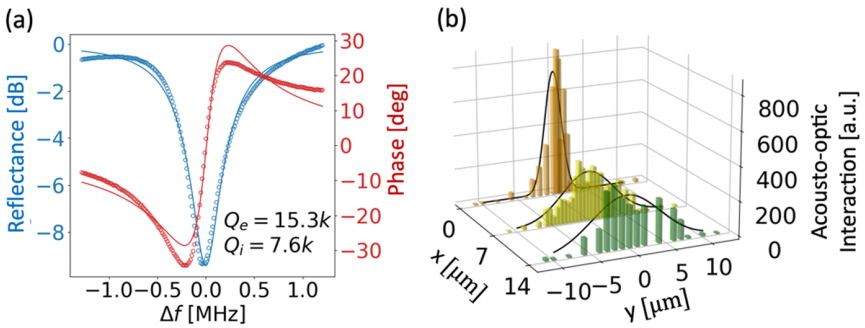

Fig. 2. (a) Microwave reflection spectrum of the SAW cavity mode (open circles). The solid curves are fits to the data. (b) Optical measurement of the acoustic waist (along the y axis) inside a focusing cavity at different distances along the cavity length (x axis) (see Supplement 1). The beam center is positioned at $(x, y) = (0, 0)$. The black curves are Gaussian fits to the data at each y value. At the focus, the measured SAW waist is 2.4 μm.

Figures 1(a) and 1(b) show an illustration of our device and its scanning electron microscope (SEM) image, respectively, and the experimental setup is depicted in Fig. 1(c). Acoustic distributed Bragg reflectors (DBRs) etched into the surface of GaAs form the focusing SAW cavity, driven by a set of Nb interdigitated transducers (IDTs) inside the cavity. We use etched grooves instead of metal mirror elements [22,23] so we can tune the reflectivity of the grooves using depth. Our chosen depth of 15 nm yields a single element reflectivity twice as large as that of a metal stripe for reasonable metal thicknesses (2% versus 1%), leading to smaller mode volumes in our SAW cavities. Nb is used for the IDTs since it is superconducting at our experimental temperatures of 4 K. Both the DBR and IDT structures are designed for microwave frequencies around 3.6 GHz and are fabricated on a wafer with epitaxially grown InAs QDs with a characteristic photon emission rate of $2\pi \times 200$ MHz. We perform a reflection measurement of an acoustic mode at 4 K in Fig. 2(a), showing a reflectance dip of ~ 9 dB on resonance. Fits to the measured microwave reflection yield an internal (external) quality factor of $Q_i = 7.6 \pm 0.1$ k ($Q_e = 15.3 \pm 0.3$ k), demonstrating efficient electro–acoustic conversion. At this temperature, the thermal occupation of the cavity mode is 30 phonons.

For acousto-optic characterization of the device, we shine tightly focused non-resonant light ($\lambda = 632$ nm) at different positions inside the SAW cavity, and measure the QD ensemble emission using a spectrometer with and without a microwave drive at the SAW cavity mode frequency. As the SAWs modulate the QD transitions, the QD spectrum spreads and the sharp transition lines broaden (see Supplement 1). We develop a simple metric to quantify this spreading at each position and map the

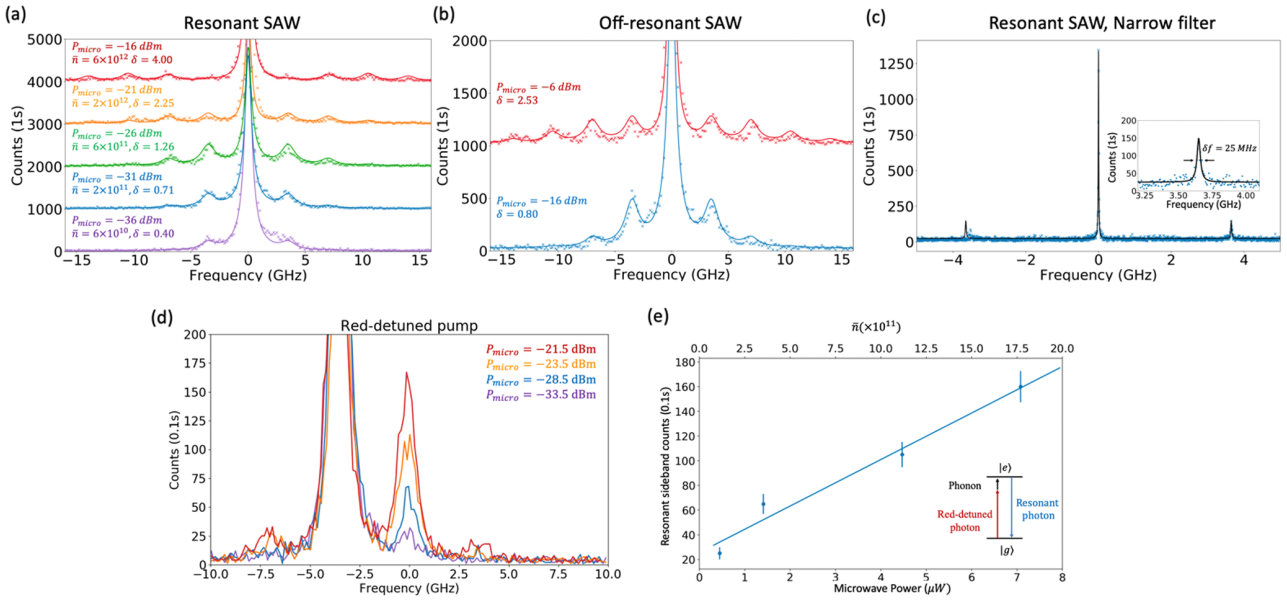

Fig. 3. (a), (b) Modulation of resonantly scattered light when driving the SAW cavity (a) on resonance and (b) off resonance, with varying microwave powers. The x axis is centered at the QD transition frequency. The center peaks are mostly due to residual pump photons. P_{micro} is the microwave input power driving the IDT, and δ is the modulation index. The data for different P_{micro} are offset in the vertical direction for clarity. The solid curves are fits to the data, considering that the modulation index scales as $\sqrt{P_{\mathrm{micro}}}$. The microwave frequency in (b) is 2 MHz off resonance from the cavity mode. The slight asymmetry in the modulation spectra is due to mismatch between the pump light and QD transition frequency, similar to optical cavities [25]. (c) Center and first two sideband peaks scanned with a narrower filter (25 MHz linewidth), showing sub-natural sideband linewidths. The asymmetry in the position and counts of the sidebands is due to temperature fluctuations of the filter over the course of the measurement. (d) Optical pump red-detuned by one SAW frequency. The large peak at −3.6 GHz is mostly due to residual pump photons. We see strong asymmetry in the sidebands, indicating that the photon scattering process on average removes phonons from the SAW cavity. (e) Resonant scattering counts for red-detuned optical pumping, as a function of input microwave power. The inset shows the dominant single-phonon scattering events. $\bar{n}$ in (a), (e) indicates the steady-state phonon number in the SAW cavity for various P_{micro}'s (see Supplement 1).

SAW cavity mode using QDs as local strain gauges [Fig. 2(b)] (see Supplement 1). The acoustic waist measured for the device shown in Fig. 1(b) is 4.6 μm, in agreement with the designed value (see Supplement 1). In Fig. 2(b), we measure a different device with a narrower SAW waist, where scans at different x positions along the cavity length confirm the focusing profile of the SAW cavity mode. We then focus our attention on individual QDs at the acoustic waist of the cavity, where the acousto-optic interaction is the strongest. A single QD transition is isolated and pumped resonantly, while the SAW cavity is driven at the cavity mode frequency with different microwave powers. Phonons modulate the photons scattered from the QD, shifting their frequency by increments of the SAW frequency [15]. We use a cross-polarization setup to reject the scattered pump photons by at least six orders of magnitude [24], and use a tunable Fabry–Perot filter (600 MHz linewidth) and a superconducting nanowire single-photon detector (SNSPD) to measure the spectrum of the scattered photons [Fig. 3(a)]. The single photons detected to the red (blue) side of the resonant laser herald phonons being added to (subtracted from) the SAW cavity. The spectra were fit to obtain the microwave power-dependent modulation index, δ. We extract a V_π of 44 mV, comparable to the state-of-the-art modulators [6,8,10,26], which range between 20 and 800 mV. This low V_π is a result of the strong electro–acoustic coupling afforded by the SAW cavity, followed by efficient photon–phonon coupling mediated by the QD.

To demonstrate the SAW cavity-enhanced aspect of the interactions, we repeat the experiment while driving SAWs at a frequency 2 MHz away from the cavity mode, which leads to a V_π of 220 mV, five times higher than that for the cavity-enhanced process [Fig. 3(b)]. The lower V_π when driving the cavity mode is due to improved impedance matching of the IDT–cavity system, as well as enhanced acousto–optic coupling due to the SAW confinement and finesse of the cavity ($\mathcal{F} = 14$). We calculate a single-phonon coupling rate of $g_0 = 2\pi \times 3.0$ kHz from the modulation index and the measured microwave coupling efficiency (see Supplement 1). This modest value results from the QDs being 750 nm below the surface where the strain field of the SAWs is relatively small (see Supplement 1) [17]. An improved value of $g_0 = 2\pi \times 42$ kHz is obtained from a device with QDs located closer to the surface at 150 nm depth.

Next, we show that, as required for quantum transduction, the coherence properties of scattered photons are likely determined by that of the acoustic mode and the pump laser, and not by incoherent emission from the QD. Resonant scattering from QDs for low pump powers follows the linewidth of the laser, not that of the QD [21]. Indeed, using a much narrower tunable filter (25 MHz linewidth), we observe sideband linewidths that are equal to that of the filter [Fig. 3(c)], confirming that our sidebands are much narrower than the natural lifetime-imposed limit of our two-level system and that we are operating below the saturation level of the QD. By increasing the optical pump power, however, incoherent emission with the linewidth of the QD lifetime ($\sim 2\pi \times 200$ MHz) can become the dominant channel. Narrow-linewidth sidebands indicate that they can be filtered rigorously for low-noise quantum transduction purposes. Additionally, due to the multimode nature of our SAW cavity, a coherent superposition of two or more cavity modes can be used and filtered simultaneously, giving our device the ability to transduce frequency qubits

[27]. We also note that our QDs are single-photon emitters, and our device is a source of modulated *single photons* [28,29] that can be readily used for quantum communications protocols.

To show single-phonon transduction, we red-detune the laser by one SAW frequency. As we operate in the resolved sideband regime, we can tune the microwave power such that the dominant process is the absorption of a single phonon and thus emission of a resonant photon [Fig. 3(d)]. The asymmetry in the scattered spectrum with respect to the pump frequency shows that, on average, scattered photons have a higher energy than pump photons, hence subtracting phonons from the cavity in the process. We note that for higher microwave powers, the scattered spectrum for a red-detuned pump becomes symmetric with respect to the QD transition, as shown in [17]. In the limit of low microwave power as used in this measurement, however, the scattering resonant with the QD transition is enhanced. Indeed, we observe that the resonant photon counts scale linearly with the SAW power [Fig. 3(e)] in this low-power regime, verifying that only one phonon is involved in the scattering process. From Fig. 3(e), we can calculate the total efficiency of detecting an optical photon upon driving the SAW cavity with a single microwave photon, yielding $\eta = 10^{-15}$. We can enhance η in the future by creating open photonic structures around the QD [30,31], optimizing the position of the QDs in the SAW's standing-wave field [17], controlling the charge state of the QD [32], and fabricating SAW cavities with smaller mode volumes (see Supplement 1).

In conclusion, we have integrated superconducting electrical circuits, SAW resonators, and quantum emitters into a single device to generate efficient electro–optic interactions, and observed strong gigahertz-regime modulation of single photons. These preliminary results open the door for demonstrations such as quantum transduction, sideband cooling [7,33] of an acoustic cavity mediated by a quantum emitter, and photon–phonon entanglement generation [34].

Funding. National Research Council; National Institute of Standards and Technology.

Acknowledgment. The authors thank John Teufel and Konrad Lehnert for fruitful discussions, and Varun Verma for fabrication of the superconducting nanowire single-photon detector. The authors also thank Adam McCaughan for providing the Python layout design code PHIDL.

Disclosures. Poolad Imany is affiliated with Icarus Quantum Inc.

Data availability. Data underlying the results presented in this paper are not publicly available at this time but may be obtained from the authors upon reasonable request.

Supplemental document. See Supplement 1 for supporting content.

[†]These authors contributed equally to this Letter.

REFERENCES

1. C. Wang, M. Zhang, X. Chen, M. Bertrand, A. Shams-Ansari, S. Chandrasekhar, P. Winzer, and M. Lončar, Nature **562**, 101 (2018).
2. X. Xu, M. Tan, B. Corcoran, J. Wu, A. Boes, T. G. Nguyen, S. T. Chu, B. E. Little, D. G. Hicks, R. Morandotti, A. Mitchell, and D. J. Moss, Nature **589**, 44 (2021).
3. M. Mirhosseini, A. Sipahigil, M. Kalaee, and O. Painter, Nature **588**, 599 (2020).
4. C.-L. Zou, H. X. Tang, L. Jiang, W. Fu, X. Han, H. X. Tang, and H. X. Tang, Optica **8**, 1050 (2021).
5. L. Fan, C. L. Zou, R. Cheng, X. Guo, X. Han, Z. Gong, S. Wang, and H. X. Tang, Sci. Adv. **4**, eaar4994 (2018).
6. K. C. Balram, M. I. Davanço, J. D. Song, and K. Srinivasan, Nat. Photonics **10**, 346 (2016).
7. M. Forsch, R. Stockill, A. Wallucks, I. Marinković, C. Gärtner, R. A. Norte, F. van Otten, A. Fiore, K. Srinivasan, and S. Gröblacher, Nat. Phys. **16**, 69 (2019).
8. W. Jiang, C. J. Sarabalis, Y. D. Dahmani, R. N. Patel, F. M. Mayor, T. P. McKenna, R. van Laer, and A. H. Safavi-Naeini, Nat. Commun. **11**, 1166 (2020).
9. A. P. Higginbotham, P. S. Burns, M. D. Urmey, R. W. Peterson, N. S. Kampel, B. M. Brubaker, G. Smith, K. W. Lehnert, and C. A. Regal, Nat. Phys. **14**, 1038 (2018).
10. L. Shao, M. Yu, S. Maity, N. Sinclair, L. Zheng, C. Chia, A. Shams-Ansari, C. Wang, M. Zhang, K. Lai, and M. Lončar, Optica **6**, 1498 (2019).
11. N. Zhu, X. Zhang, X. Zhang, X. Han, X. Han, C.-L. Zou, C.-L. Zou, C. Zhong, C. Zhong, C.-H. Wang, C.-H. Wang, L. Jiang, L. Jiang, and H. X. Tang, Optica **7**, 1291 (2020).
12. H.-T. Tu, K.-Y. Liao, Z.-X. Zhang, X.-H. Liu, S.-Y. Zheng, S.-Z. Yang, X.-D. Zhang, H. Yan, and S.-L. Zhu, Nat. Photonics **16**, 291 (2022).
13. K. J. Satzinger, Y. P. Zhong, H. S. Chang, G. A. Peairs, A. Bienfait, M. H. Chou, A. Y. Cleland, C. R. Conner, É. Dumur, J. Grebel, I. Gutierrez, B. H. November, R. G. Povey, S. J. Whiteley, D. D. Awschalom, D. I. Schuster, and A. N. Cleland, Nature **563**, 661 (2018).
14. S. Maity, L. Shao, S. Bogdanović, S. Meesala, Y. I. Sohn, N. Sinclair, B. Pingault, M. Chalupnik, C. Chia, L. Zheng, K. Lai, and M. Lončar, Nat. Commun. **11**, 193 (2020).
15. D. Wigger, H. J. Krenner, J. J. Finley, K. Müller, M. Weiß, M. Nägele, P. Machnikowski, T. Kuhn, P. Machnikowski, and H. J. Krenner, Optica **8**, 291 (2021).
16. E. D. S. Nysten, A. Rastelli, and H. J. Krenner, Appl. Phys. Lett. **117**, 121106 (2020).
17. M. Metcalfe, S. M. Carr, A. Muller, G. S. Solomon, and J. Lawall, Phys. Rev. Lett. **105**, 037401 (2010).
18. M. J. A. Schuetz, E. M. Kessler, G. Giedke, L. M. K. Vandersypen, M. D. Lukin, and J. I. Cirac, Phys. Rev. X **5**, 031031 (2015).
19. D. Wigger, M. Weiß, M. Lienhart, K. Müller, J. J. Finley, T. Kuhn, H. J. Krenner, and P. Machnikowski, Phys. Rev. Res. **3**, 033197 (2021).
20. J. Chan, A. H. Safavi-Naeini, J. T. Hill, S. Meenehan, and O. Painter, Appl. Phys. Lett. **101**, 081115 (2012).
21. C. Matthiesen, A. N. Vamivakas, and M. Atatüre, Phys. Rev. Lett. **108**, 093602 (2012).
22. M. E. Msall and P. V. Santos, Phys. Rev. Appl. **13**, 014037 (2020).
23. B. A. Moores, L. R. Sletten, J. J. Viennot, and K. W. Lehnert, Phys. Rev. Lett. **120**, 227701 (2018).
24. A. V. Kuhlmann, J. Houel, D. Brunner, A. Ludwig, D. Reuter, A. D. Wieck, and R. J. Warburton, Rev. Sci. Instrum. **84**, 073905 (2013).
25. M. Zhang, B. Buscaino, C. Wang, A. Shams-Ansari, C. Reimer, R. Zhu, J. Kahn, and M. Lončar, Nature **568**, 373 (2019).
26. Y. Tsuchimoto, Z. Sun, E. Togan, S. Fält, W. Wegscheider, A. Wallraff, K. Ensslin, A. İmamoğlu, and M. Kroner, "Large-bandwidth transduction between an optical single quantum-dot molecule and a superconducting resonator," arXiv:2110.03230v1 (2021).
27. J. M. Lukens and P. Lougovski, Optica **4**, 8 (2017).
28. M. Weiß, S. Kapfinger, T. Reichert, J. J. Finley, A. Wixforth, M. Kaniber, and H. J. Krenner, Appl. Phys. Lett. **109**, 033105 (2016).
29. B. Villa, A. J. Bennett, D. J. P. Ellis, J. P. Lee, J. Skiba-Szymanska, T. A. Mitchell, J. P. Griffiths, I. Farrer, D. A. Ritchie, C. J. B. Ford, and A. J. Shields, Appl. Phys. Lett. **111**, 011103 (2017).
30. L. Sapienza, M. Davanço, A. Badolato, and K. Srinivasan, Nat. Commun. **6**, 7833 (2015).
31. R. A. DeCrescent, Z. Wang, P. Imany, R. C. Boutelle, R. P. Mirin, and K. L. Silverman, "Semicircular dielectric gratings for strongly polarized and enhanced emission from GaAs/InAs quantum dots," in *Conference on Lasers and Electro-Optics (CLEO)* (2022).
32. N. Tomm, A. Javadi, N. O. Antoniadis, D. Najer, M. C. Löbl, A. R. Korsch, R. Schott, S. R. Valentin, A. D. Wieck, A. Ludwig, and R. J. Warburton, Nat. Nanotechnol. **16**, 399 (2021).
33. J. D. Teufel, T. Donner, D. Li, J. W. Harlow, M. S. Allman, K. Cicak, A. J. Sirois, J. D. Whittaker, K. W. Lehnert, and R. W. Simmonds, Nature **475**, 359 (2011).
34. N. Fiaschi, B. Hensen, A. Wallucks, R. Benevides, J. Li, T. P. M. Alegre, and S. Gröblacher, Nat. Photonics **15**, 817 (2021).